A Novel Paradigm for the Qualitative Synthesis of Simple Kinematic Chains Based on Complexity Measures

TR-CIM-10-02

W.A. Khan and J. Angeles
Department of Mechanical Engineering &
Centre for Intelligent Machines, McGill University,
Montreal, Quebec, H3A 2K6, Canada

January, 2010

Contents

List of Figures

List of Tables

Abstract

Proposed in this paper is a paradigm for the qualitative synthesis of *simple kinematic chains* that is based on the concept of complexity. Qualitative synthesis is understood here as the *number* and the *type* stages of the kinematic-synthesis process. The formulation hinges on the geometric complexity of the surface associated with lower kinematic pairs. First, the geometric complexity of curves and surfaces is defined via the *loss of regularity* (LOR). The LOR, based in turn on the concept of *diversity*, measures the spectral richness of the curvature of either the curve or the surface under study. A complete procedure to obtain the LOR by means of Fourier expansion and Parseval's equality is introduced. As examples, the LOR of various closed curves is evaluated. Next, the LOR of surfaces associated with the one-dof lower kinematic pairs is discussed. The paper closes with a complexity analysis of all six lower kinematic pairs, as a means to guide the mechanical designer into the conceptual stage of the design process. The paradigm is illustrated with the computation of the complexity of the four-bar linkage in all its versions, planar, spherical and spatial, as well as that of a transmission for the conversion of a rotation about a vertical axis into one about a horizontal axis.

1   Introduction

According to Hartenberg and Denavit (1964), the kinematic synthesis of linkages is a process that comprises three successive stages, namely, a) *number synthesis*, b) *type synthesis*, and c) *dimensional synthesis*. In stage a) the machine designer decides how many links and joints the kinematic chain will comprise; in b) a decision is made on what kinds of joints will compose the chain; in c) the link dimensions are calculated so as to satisfy the machine-design task at hand. The paradigm developed here aims at stages a) and b) of the synthesis process. Stage c), essentially quantitative, has been extensively studied in the literature since the works of Burmester (1886) and Freudenstein (1955). The paradigm is based on the concept of *complexity*.

Prior to introducing the complexity of kinematic chains, the one associated with kinematic pairs is discussed. The latter is based, in turn, on the concept of complexity of the surface common to the single-dof lower kinematic pairs (LKPs), whence the complexity of all six LKPs is derived.

Several complexity measures of 3D surfaces are available in the literature. These measures stem from a variety of fields, such as computer graphics, metrology, biology, chemistry, etc. The complexity measures in computer graphics (Rossignac, 2005) are based on the *algorithmic complexity* of 3D shapes. Algorithmic complexity is, broadly speaking, an index that represents computational resources, in terms of the computation time (Garey and Johnson, 1979; Walsh, 1998) and the size of the program required to generate a representation of the given surface (Li and Vitányi, 1997).

Another pertinent type is *morphological complexity*. This type determines the regularity and smoothness of a given surface. These complexity measures are based on surface curvature (Koenderink, 1990).

While some of these measures provide a bound on the complexity of the surfaces under study, others provide an index that is local to the surface. For these reasons, the complexity measures available are not useful for the mechanical designer.

This paper provides a formal account on the complexity measure introduced by Khan et al. (2006). The measure is a *global index*, intended to assess "how far" a given surface lies from the *simplest* of all surfaces, regardless of its dimensions, namely, the *sphere*. In this vein, the index is first introduced for planar curves and then extended to 3D surfaces. Several propositions are then discussed and complemented by examples.

The complexity of the *lower kinematic pairs* is evaluated in Section 9. This section is intended to support the conceptual design of mechanical systems. In the mechanical design literature, a pivot is usually preferred over a slide (Chakrabarti, 2002), a rule that comes from intuition and experience, more so than from analysis. This paper is an attempt to provide a theoretical framework that, among other objectives, will help justify this rule. The focus here is on *simple kinematic chains*, more general chains being the subject of a forthcoming paper. A simple kinematic chain is understood, within the theory of kinematic chains, as a chain whose links are coupled to only one other link—the case of single links—or, at most, to two other links—the case of binary links. Ternary, quaternary and *higher-order links* occur in more general

kinematic chains, with either tree- or multi-loop structures.

2   Geometric Complexity of Contours

The concepts described in this section were outlined in a previous paper (Khan et al. , 2006). Here we expand on these concepts, introducing some pertinent propositions and their proofs.
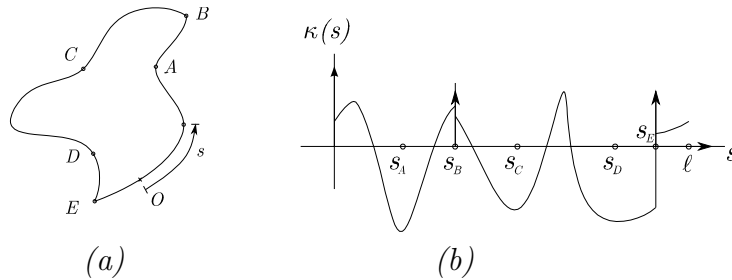
Figure 1: (a) A contour with two singular points and (b) its curvature distribution

A planar contour $\mathcal{C}$ of a fairly general shape is illustrated in Fig. 1(a), with singular points[1] B and E, and concavities at points A, C and D. The curvature $\kappa(s)$ is defined as

$$\kappa(s) = \frac{d\phi}{ds} \tag{1}$$

where ϕ is the angle made by the tangent to $\mathcal{C}$ with a fixed direction, and s is the arc length. We illustrate in Fig. 1(b) the curvature distribution of $\mathcal{C}$, which attains unbounded values at the singular points B and E. The curvature at the singular points is thus indicated with an arrow pointing upward, to hint the presence of a Dirac function.

2.1   Loss of Regularity of Planar Curves

We introduce first the geometric complexity of a contour based on its curvature diversity, i.e., on the spectral richness of its curvature and its derivative with respect to the dimensionless parameter $\sigma = s/l$, with s indicating the arc length from a given reference point and l the contour length. Curvature is a plausible indicator of *shape complexity* because it is invariant under rigid-body motions. Notice that point coordinates are not suitable because these are sensitive to translations, while tangent-direction is sensitive to rotations of the contour.

---

[1]A point on a plane curve is called *singular* if two or more branches of the same curve meet. If the tangents at the meeting point are distinct, the point is called a *node*; if the tangents coincide, the point is called a *cusp* (Gibson, 1998).

Borrowing from Taguchi's *loss function* in the realm of *robust engineering* (Taguchi, 1993), we define the *loss of regularity*, abbreviated LOR, as[2]

$$LOR \equiv \frac{||\kappa'(\sigma)||_2}{||\kappa(\sigma)||_2} \tag{2}$$

where $\kappa(\sigma)$ is the curvature of the curve and $\kappa'(\sigma)$ is its derivative with respect to σ. The LOR is dimensionless, its numerator and denominator being the rms values of κ' and κ, respectively, i.e.,

$$||\kappa(\sigma)||_2^2 = \int_0^1 [\kappa(\sigma)]^2 \, d\sigma, \quad ||\kappa'(\sigma)||_2^2 = \int_0^1 [\kappa'(\sigma)]^2 \, d\sigma \tag{3}$$

Notice that the LOR must be evaluated w.r.t. the *preferred* parameter σ defined above. However, the expressions for the curvature and its derivative may conveniently be expressed in another parameter $t \in [t_0, t_1]$. For this case, the computation of the LOR should change accordingly, as shown below.

Let $s = s(t)$ be the length of the curve, s' its derivative with respect to t, i.e. $s' = ds/dt$, and l the total length of the curve. Then

$$\sigma(t) = \frac{1}{l}s(t) \Rightarrow d\sigma = \frac{1}{l}ds \quad \text{and} \quad \sigma'(t) \equiv \frac{d\sigma}{dt} = \frac{1}{l}s'(t) \tag{4}$$

with primes indicating differentiation with respect to t. The LOR in terms of the parameter t is then given by

$$LOR = \left[\frac{\int_{t_0}^{t_1} \left(\frac{\partial \kappa(t)}{\partial(t)} \frac{\partial t}{\partial \sigma}\right)^2 \frac{1}{l} s' dt}{\int_{t_0}^{t_1} \kappa(t)^2 \frac{1}{l} s' dt} \right]^{1/2} = l \left[\frac{\int_{t_0}^{t_1} [\kappa'(t)^2/s'] dt}{\int_{t_0}^{t_1} \kappa(t)^2 s' dt} \right]^{1/2} \tag{5}$$

Evaluating the numerator and the denominator of eq.(2) is, in general, far from trivial. However, notice that $\kappa(\sigma)$ is periodic over the σ-axis, of period 1. We thus resort to the Fourier series of $\kappa(\sigma)$, thus obtaining

$$\kappa(\sigma) = a_0 + \sum_{k=1}^{\infty} [a_k \cos(2\pi n\sigma) + b_k \sin(2\pi n\sigma)] \tag{6}$$

where

$$a_0 = \int_0^1 \kappa(\sigma) d\sigma, \quad a_k = 2\int_0^1 \kappa(\sigma)\cos(2\pi n\sigma) d\sigma, \quad b_k = 2\int_0^1 \kappa(\sigma)\sin(2\pi n\sigma) d\sigma \tag{7}$$

Differentiating eq.(6) with respect to σ, we obtain

$$\kappa'(\sigma) = 0 + \sum_{k=1}^{\infty} [c_k \cos(2\pi k\sigma) + d_k \sin(2\pi k\sigma)] \tag{8a}$$

---

[2]We denote with $|| \cdot ||_2$ the 2-norm in a *space of functions* (Courant and Hilbert, 1953).

where

$$c_k = 2\pi k b_k, \quad d_k = -2\pi k a_k \tag{8b}$$

Next we resort to *Parseval's equality* (Strang, 1986) to obtain the 2-norm, as required in eq.(2), in the "frequency" domain,

$$\|\kappa(\sigma)\|_2^2 \equiv \int_0^1 |\kappa(\sigma)|^2 d\sigma = a_0^2 + \frac{1}{2}\sum_{k=1}^{\infty}(a_k^2 + b_k^2) \tag{9}$$

$$\|\kappa'(\sigma)\|_2^2 \equiv \int_0^1 |\kappa'(\sigma)|^2 d\sigma = 0 + \frac{1}{2}\sum_{k=1}^{\infty}(c_k^2 + d_k^2) \tag{10}$$

Substituting the values of $\|\kappa(\sigma)\|_2^2$ and $\|\kappa'(\sigma)\|_2^2$ from eqs.(9) and (10) into eq.(2), we obtain the general form of the LOR, in the frequency domain, namely,

$$LOR = 2\pi \left(\frac{\sum_{k=1}^{\infty} k^2(a_k^2 + b_k^2)}{2a_0^2 + \sum_{k=1}^{\infty}(a_k^2 + b_k^2)} \right)^{1/2} \tag{11}$$

which is the expression sought. Hence, all we need, to evaluate the LOR, are the coefficients a_0, a_k and b_k of the Fourier expansion of the curvature $\kappa(\sigma)$.

Lemma 1 *Assume that the curvature of a closed curve is periodic and repeats itself m times within the curve. The LOR of the curve is m-times the LOR evaluated for one period[3].*

2.2   Comparison of LOR and the Coefficient of Variation

The LOR measures the *diversity* of the curvature distribution of the given curve. Diversity has been extensively used in design, with a measure thereof given by what is known as the *coefficient of variation*—see, e.g., (Shigley and Mischke, 1981). The coefficient of variation C_x, however, is not appropriate to measure the spectral richness of the curvature distribution of a geometric contour, as shown below.

Let x be a variable defined over the range $a \leq x \leq b$, whether *random* or *deterministic*[4]. The coefficient of variation C_x of x is defined as

$$C_x \equiv \frac{\hat{x}}{\overline{x}}, \quad \overline{x} \neq 0 \tag{12}$$

in which $\overline{x}$ represents the mean value of x and $\hat{x}$ the variance of x, i.e., the root-mean square value of $x - \overline{x}$. Apparently, C_x is dimensionless and can attain any real value, i.e.,

$$-\infty < C_x < +\infty \tag{13}$$

---

[3]The proof follows directly from eq.(11) if we replace k by km. Further, since m is constant for a given curve, it may be taken out of the summation, which proves the Lemma.

[4]In the reference cited above, the coefficient of variation C_x of x is defined under the assumption that x is random, but this need not be the case.

Furthermore, the coefficient of variation is defined also for discrete variables. Assume that the variable x takes on the discrete set of numerical values $\{\, x_i \,\}_1^m$. In this case,

$$\overline{x} \equiv \frac{1}{m}\sum_1^m x_i, \quad \hat{x} \equiv \sqrt{\frac{1}{m}\sum_1^m (x_i - \overline{x})^2} \qquad (14a)$$

the coefficient of variation being defined in exactly the same way as in eq.(12).

The coefficient of variation of the curvature (CVC) of $\mathcal{C}$ is thus the ratio $C_\kappa = \hat{\kappa}/\overline{\kappa}$. The mean $\overline{\kappa}$ and the variance $\hat{\kappa}$ of $\kappa(\sigma)$ are readily computed as

$$\overline{\kappa} = \int_0^1 \kappa(\sigma)d\sigma, \quad \hat{\kappa} = \sqrt{\int_0^1 [\kappa(\sigma) - \overline{\kappa}]^2 d\sigma} \qquad (15)$$

Since the contour is a closed curve, $\overline{\kappa}$ is bound to be positive, and hence, its coefficient of variation is positive as well.

Using Parseval's equality, $\overline{\kappa}$ and $\hat{\kappa}$ may be readily obtained as

$$\overline{\kappa} = a_0, \quad \hat{\kappa} = \sqrt{\frac{1}{2}\sum_{k=1}^\infty (a_k^2 + b_k^2)} \qquad (16)$$

and hence,

$$C_\kappa = \frac{1}{4}\left(\frac{\sum_{k=1}^\infty (a_k^2 + b_k^2)}{a_0^2}\right)^{1/2} \qquad (17)$$

Notice that the CVC of two contours $\mathcal{C}_1$ and $\mathcal{C}_2$ with harmonic curvature distributions, $\kappa_1(s) = \overline{\kappa} + \kappa_0 \cos(2\pi\omega_0\sigma)$ and $\kappa_2 = \overline{\kappa} + \kappa_0 \cos(2N\pi\omega_0\sigma)$, where N is a "large" integer, are identical, which is not acceptable. One way to overcome this problem could be to resort to the coefficient of variation of the rate of change of curvature, $\kappa'(\sigma)$. However, a quick glance at eq.(8a) reveals that the mean value $\overline{\kappa}'(\sigma)$ is zero, and hence the coefficient of variation $C_{\kappa'}$ cannot be evaluated. The coefficient of variation is thus not useful for our application.

3   Geometric Complexity of Surfaces

In this section we will extend the concept of LOR to 3-D surfaces $\mathcal{M}$. Surfaces are characterized, at any point P on the surface, by two curvatures, known as the principal curvatures κ_{max} and κ_{min}. Two well-known properties derived from the principal curvatures are the Gaussian curvature K and the mean curvature H, defined as

$$K \equiv \kappa_{min}\kappa_{max}$$
$$H \equiv (\kappa_{min} + \kappa_{max})/2$$

Neither K nor H can effectively indicate the curvature distribution. Instead, we propose to use the *local* root-mean-square of the principal curvatures κ_{rms}, i.e.,

$$\kappa_{rms} \equiv \sqrt{\frac{1}{2}(\kappa_{max}^2 + \kappa_{min}^2)} \tag{18}$$

In differential geometry, a surface is characterized locally by the linear *shape operator*[5] $\mathcal{S}$. Let $\mathcal{T}$ be the plane tangent to the surface $\mathcal{M}$ at point P and $\mathbf{u}$ be the unit vector normal to $\mathcal{T}$ stemming from P. The shape operator maps any vector $\mathbf{v} \in \mathcal{T}$ into the directional derivative of $\mathbf{u}$ in the $\mathbf{v}$-direction, i.e. $\mathcal{S} : \mathcal{T} \to \mathcal{T}$, $\mathcal{S}(\mathbf{v}) = -\nabla_{\mathbf{v}}\mathbf{u} \equiv -(\nabla\mathbf{u})\mathbf{v}/\|\mathbf{v}\| \equiv -d\mathbf{u}/dv$, where v is a coordinate defined in the direction of $\mathbf{v}$.

Let $\mathbf{S}$ be a *shape matrix* representing $\mathcal{S}$ with respect to a suitable basis. The three curvatures introduced earlier, namely K, H and κ_{rms}, may be evaluated from $\mathbf{S}$ as

$$K = \det(\mathbf{S}), \quad H = \frac{1}{2}\mathrm{tr}(\mathbf{S}) \quad \text{and} \quad \kappa_{rms} = ||\mathbf{S}||_F = \sqrt{\frac{1}{2}\mathrm{tr}(\mathbf{S}\mathbf{S}^T)} \tag{19}$$

where $|| \cdot ||_F$ is the *matrix weighted Frobenius norm*, with a weighting matrix $\mathbf{W} = (1/2)\,\mathbf{1}$, $\mathbf{1}$ being the 2×2 identity matrix.

Further, since a surface has two degrees of freedom, we need to evaluate the loss of regularity with respect to two normalized parameters, σ_1 and σ_2. The choice of these parameters is arbitrary. However, as we will see presently, for most "engineering surfaces", a natural choice of σ_1 and σ_2 always exists.

We define the LOR of a surface as

$$LOR \equiv \left[\frac{\int_0^1 \int_0^1 [(\partial\kappa_{rms}/\partial\sigma_1)^2 + (\partial\kappa_{rms}/\partial\sigma_2)^2]d\sigma_1 d\sigma_2}{\int_0^1 \int_0^1 \kappa_{rms}^2 d\sigma_1 d\sigma_2} \right]^{1/2} \tag{20}$$

Proposition 1 *The LOR of an extruded surface, obtained by sweeping a planar generatrix $\mathcal{G}$, is identical to the LOR of $\mathcal{G}$.*

Proof: Figure 2 shows an extruded surface with a "natural" choice of parameters σ_1 and σ_2. Apparently, in the direction of extrusion, given by the unit vector $\mathbf{e}$, and along which σ_2 is measured, the surface has a constant curvature $\kappa_2 = 0$. Moreover, the curvature of the surface, along the direction in which σ_1 is measured, is independent of σ_2. As a consequence, these two directions are the principal directions of curvature, and hence, $\kappa_{rms}(\sigma_1, \sigma_2) = |\kappa_{\mathcal{G}}(\sigma_1)|$, where $\kappa_{\mathcal{G}}$ is the curvature at the corresponding point on the generatrix $\mathcal{G}$. Therefore, the LOR of the surface under study simplifies to

$$LOR = \left[\frac{\int_0^1 (\partial\kappa_{rms}/\partial\sigma_1)^2 d\sigma_1}{\int_0^1 \kappa_{rms}^2 d\sigma_1} \right]^{1/2} \tag{21}$$

---

[5]The reader is referred to any elementary differential geometry text for details on the shape operator
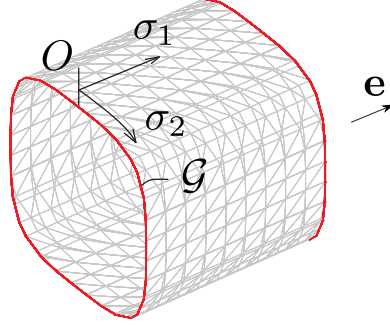
Figure 2: An extruded surface

From elementary differential geometry, the two principal curvatures at any point of an extruded surface are $\kappa_{\mathcal{G}}$ and 0. Hence, the LOR of the surface under study is dependent solely on $\kappa_{\mathcal{G}}$, i.e.,

$$LOR = \left[\frac{\int_0^1 (\partial \kappa_{\mathcal{G}}/\partial \sigma_1)^2 d\sigma_1}{\int_0^1 \kappa_{\mathcal{G}}^2 d\sigma_1}\right]^{1/2} = \frac{||\kappa'_{\mathcal{G}}(\sigma_1)||_2}{||\kappa_{\mathcal{G}}(\sigma_1)||_2} \qquad (22)$$

which is the LOR of the generatrix $\mathcal{G}$.

Proposition 2 *The LOR of a surface of revolution is simply the LOR of the surface evaluated along its generatrix*
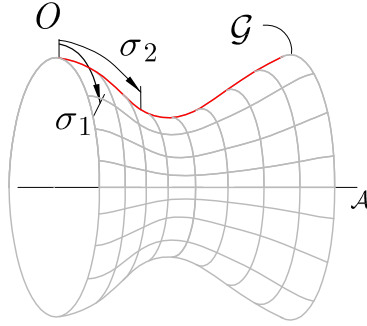
Figure 3: A surface of revolution

Proof: Figure 3 shows a surface with a "natural" choice of parameters σ_1 and σ_2. The root-mean-square curvature κ_{rms} is independent of σ_1 by symmetry, and hence, $\kappa_{rms}(\sigma_1, \sigma_2) = \kappa_{rms}(\sigma_2)$. The LOR of the surface under study thus simplifies to

$$LOR = \left[\frac{\int_0^1 (\partial \kappa_{rms}/\partial \sigma_2)^2 d\sigma_2}{\int_0^1 \kappa_{rms}^2 d\sigma_2}\right]^{1/2} = \frac{||\kappa'_{rms}(\sigma_2)||_2}{||\kappa_{rms}(\sigma_2)||_2} \qquad (23)$$

which is the LOR of $\mathcal{G}$.

Proposition 3 *The LOR of a surface does not change under a uniform scaling*

As the proof of this proposition is straightforward, it need not be included.

4   Examples

In this section we evaluate the LOR of various planar curves.

4.1   LOR of a Circle
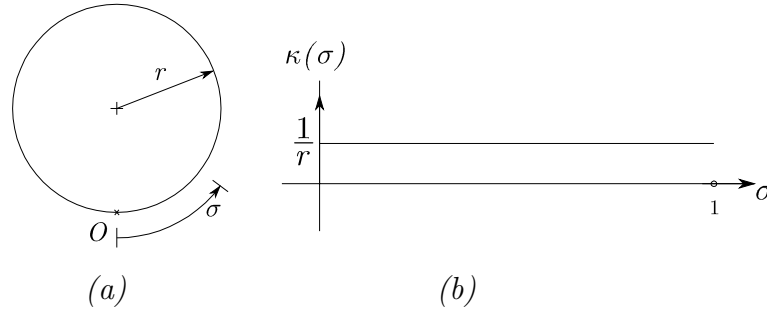
Figure 4: A circle: (a) the shape and (b) its curvature distribution

For the circle of Fig. 4a, the curvature $\kappa(\sigma)$ is constantly equal to unity. The mean curvature is thus given by

$$\overline{\kappa} = a_0 = 1$$

where r is the radius of the circle. The other coefficients, a_k, b_k, of the Fourier series expansion of $\kappa(\sigma)$ thus vanish. Substituting $a_k = b_k = 0$ into eq.(11), we obtain that $LOR = 0$, the LOR of a circle of any radius r thus vanishing, as it should.

4.2   LOR of an Equilateral Triangle

Let us consider now the equilateral triangle depicted in Fig. 5(a), of side a, its curvature distribution[6] being plotted in Fig. 5(b) vs. $\sigma = s/3a$. Notice that this shape has a curvature of zero everywhere, except for the corners, where the curvature attains infinite values, represented by *Dirac functions*, a.k.a. *impulses*, of amplitude $\sqrt{3}/2$, which is the sine of $2\pi/3$, the angle through which the geometric tangent turns at the

---

[6]The curvature distribution was found by straightforward computation of the derivative of the unit tangent with respect to the dimensionless arc length σ.
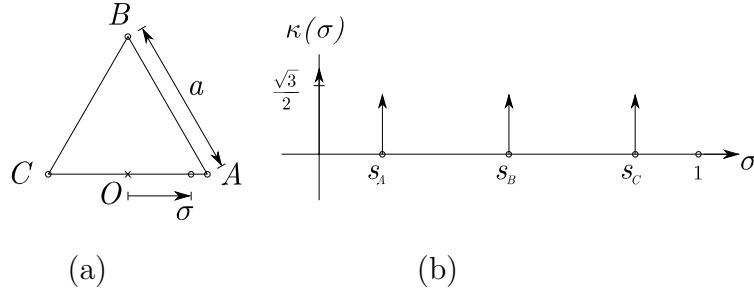
Figure 5: An equilateral triangle: (a) its parameterization and (b) its curvature distribution

corners. The calculation of the mean curvature $\overline{\kappa}$ in this case is straightforward, for the integral of a unit impulse is unity, and hence,

$$\overline{\kappa} = a_0 = \frac{3\sqrt{3}}{2} \tag{24}$$

Apparently, the curvature distribution in this case is symmetric, which means that its Fourier series has only a constant term, $\overline{\kappa}$, and cosine terms, namely,

$$\kappa(s) = \overline{\kappa} + \sum_{k=1}^{\infty} a_k \cos(2\pi k\sigma) \tag{25}$$

where

$$a_k = \sqrt{3} \left[(-1)^k + 2 \cos\left(\frac{k\pi}{3}\right) \right] \tag{26}$$

The sum of the squares of the Fourier coefficients may be expressed as

$$\sum_{k=1}^{\infty} a_k^2 = \sum_{j=1}^{\infty} a_{3j}^2 = \sum_{j=1}^{\infty} \left(3^3\right) \tag{27}$$

Substituting the values obtained in eqs.(25) and (27) into eq.(11) we obtain

$$LOR = 2\pi \left(\frac{\sum_{j=1}^{\infty}(j^2)}{1/2 + \sum_{j=1}^{\infty}(1)} \right)^{1/2} \tag{28}$$

where j is a positive integer, i.e. $j \in \mathbb{Z}^+$. Since the numerator of the above equation grows much faster than the denominator, the LOR of interest is unbounded.

The foregoing analysis illustrates a point: a contour with singular points is the most complex, while a circle the least. In-between lie contours with continuously varying curvatures, like ellipses and superellipses, as discussed below.
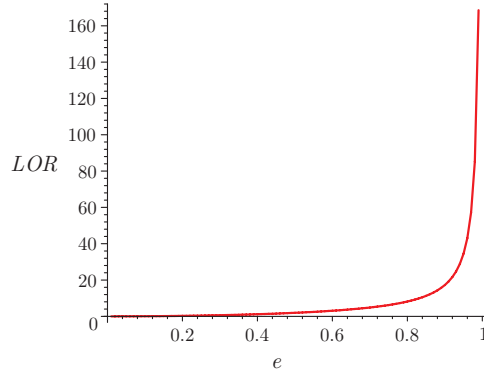
Figure 6: LOR of ellipses vs. eccentricity e

4.3   LOR of an Ellipse

The curvature of an ellipse can be expressed as

$$\kappa(t) = \frac{k_1 k_2}{(k_2^2 \cos^2 t + k_1^2 \sin^2 t)^{3/2}} \tag{29}$$

where k_1 and k_2 are the lengths of the semimajor and semiminor axes, respectively, and $t \in [0, 2\pi]$ is the parameter. Figure 6 shows a plot of the loss of regularity vs. the eccentricity e, which is defined as

$$e = \frac{\sqrt{k_1^2 - k_2^2}}{k_1}; \ k_1 \geq k_2$$

4.4   LOR of Lamé Curves

Lamé curves[7] are planar curves that can be expressed in implicit form as (Gardner, 1965)

$$\left(\frac{x}{a}\right)^p + \left(\frac{y}{b}\right)^p = 1 \tag{30}$$

where p can be any rational number while a and b are positive real numbers. There are nine different types of Lamé curves, based on the form of the exponent p. These types may be divided into two categories (Loria, 1902; Jaklič et al. , 2000), i.e., for $p > 0$ and for $p < 0$.

For our study, we resort to a subset of Lamé curves as given by

$$x^m + y^m = 1 \tag{31}$$

where m is a positive integer. When $m = 2$, the corresponding curve is a circle of unit radius with its center at the origin of the x-y plane. For even values of m, as m

---

[7]Named after the French mathematician Gabriel Lamé (1795–1870), who introduced these curves.

increases, the curve becomes flatter and flatter at its intersections with the coordinate axes, approaching a square. For $m \to \infty$, the curve is a square of sides equal to two units of length and centered at the origin.

However, for odd values of m, although the curve looks like the even case in the first quadrant, it is, in fact, an open curve with real asymptote passing through the origin and with a slope of -1. In Fig. 7, the Lamé curves for various values of m are shown.
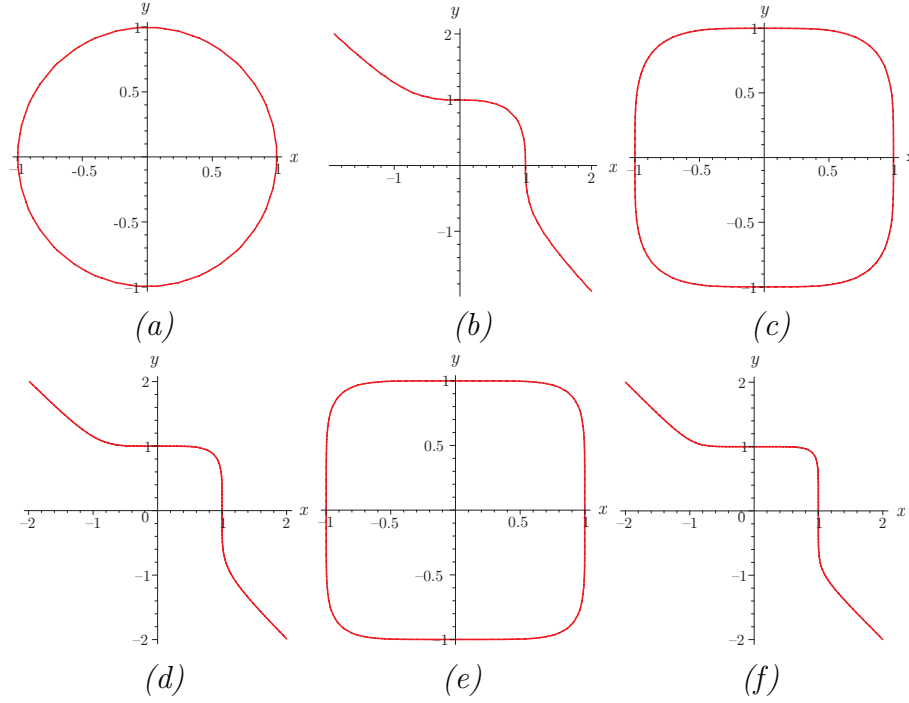
Figure 7: Lamé curves for: (a) m=2; (b) m=3; (c) m=4; (d) m=5; (e) m=6; and (f) m=7

Now, in order to obtain a closed curve for odd m as well, a slight modification may be introduced, i.e.,

$$|x|^m + |y|^m = 1 \tag{32}$$

Figure 8 shows the curves obtained using eq.(32), for $m = 2$, 3, 5, 10 and 25. When m is even, the absolute-value bars can be deleted. However, when m is odd, the bars must be kept. Absolute values, however, introduce discontinuities in the curvature because the absolute-value function is not differentiable at the origin.

The curves shown in Fig. 8 have double symmetry, and hence, it is sufficient to study only the first quadrant of the curves for the purpose of LOR analysis. Therefore, we focus our study on the algebraic curves of the form

$$f(x, y) \equiv x^m + y^m - 1 = 0; \quad 2 < m \in \mathbb{Z}, \, x, y \in \mathbb{R}^+ \tag{33}$$
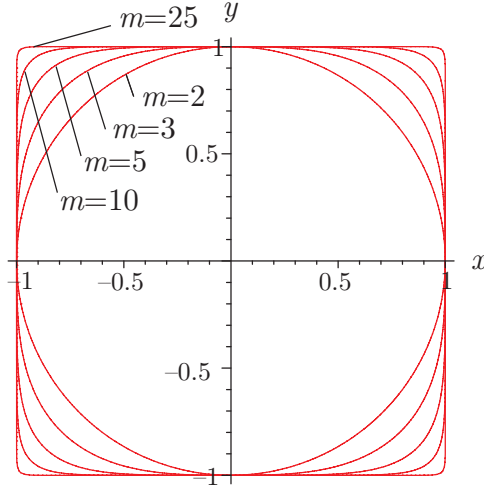
Figure 8: Lamé curves of eq.(32) for $m = 2, 3, 5, 10$ and 25

where $\mathbb{Z}$ is the set of integers. We assume that both x and y are dimensionless.

The parametric form of eq.(33) is given by

$$x(\theta) = \frac{1}{(1 + \tan^m \theta)^{1/m}}, \quad y(\theta) = \frac{\tan \theta}{(1 + \tan^m \theta)^{1/m}} \tag{34}$$

where $\theta \in [0, \pi/2]$ is the angle that a line segment between the origin O and any point P on the Lamé curve under study makes with the positive x-axis. The curvature $\kappa(\theta)$ is readily computed as

$$\kappa(\theta) = \frac{x'(\theta)y''(\theta) - y'(\theta)x''(\theta)}{(x'(\theta)^2 + y'(\theta)^2)^{3/2}} \tag{35}$$

Notice that, for $m > 2$, $\kappa(\theta)$ is undefined at $\theta = 0$ and $\pi/2$. However, this does not mean that the curvature of the curves under study is discontinuous at points $(1, 0)$ or $(0, 1)$, for we can readily verify that the limit of $\kappa(\theta)$ is zero as θ approaches 0 or $\pi/2$. Further, the curvature κ may be expressed in implicit form as

$$\kappa(x, y) = \frac{2f_{xy}f_x f_y - f_{xx}f_y^2 - f_{yy}f_x^2}{(f_x^2 + f_y^2)^{(3/2)}} \tag{36}$$

where f_x and f_{xx} are the first and second-order derivatives of f with respect to x, f_y and f_{yy} being defined likewise, and f_{xy} is the mixed second-order derivative of f. For the curve $f(x, y)$ of eq.(33), we obtain

$$\kappa(x, y) = \frac{(m - 1)(xy)^{(m-2)}(x^m + y^m)}{[x^{(2m-2)} + y^{(2m-2)}]^{3/2}} \tag{37}$$

whence it is apparent that, for $m > 2$, the curvature $\kappa(x, y)$ is zero at points $(1, 0)$ and $(0, 1)$.

The LOR is plotted vs. m in Fig. 9, which shows that the LOR increases almost linearly with m.
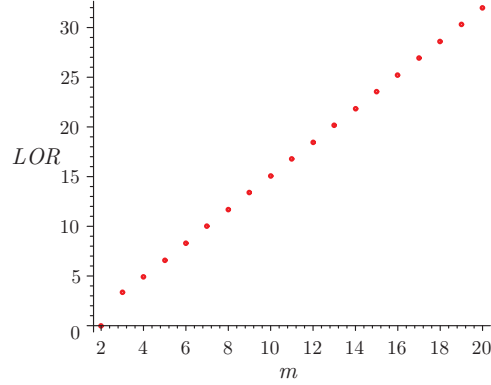
Figure 9: The LOR of the Lamé curves of eq.(33)

5 LOR of the Surfaces Associated with the Elementary LKPs

A *kinematic pair* is the coupling of two rigid bodies, called links. When the coupling takes place in such a way that the two links share a common surface, a *lower kinematic pair* (LKP) results; when the coupling takes place along a common line or a common point, a *higher kinematic pair* (HKP) is obtained. Examples of HKPs include gears and cams, the paper focusing on lower pairs.

There are six lower kinematic pairs, namely, revolute R, prismatic P, helical H, cylindrical C, planar F, and spherical S. The six LKPs are classified, for the purposes of this paper, into two types, *elementary* and *composite*, the former being those with one single dof, the latter those with a dof of two and three. The elementary LKPs are, thus the revolute, the prismatic and the helical or screw pairs.

In this section we derive the LOR of the surfaces associated with the elementary lower kinematic pairs. The LOR then leads to the concept of *shape complexity* of all six LKPs.

A general method to verify whether a certain shared surface between two links would result in a lower kinematic pair is available in Voinea and Stroe (1995)[8].

5.1 LOR of the Surface of the R Pair

Typically, the surface associated with the revolute pair is assumed to be a cylinder. However, in order to realize this pair, the translation in the axial direction of the cylindrical surface must be constrained. This calls for an alternative surface, labeled $\mathcal{S}_{\mathrm{R}}$, which must then be blended smoothly with a cylindrical surface—that of a connecting shaft—in order to avoid curvature discontinuities.

The above discussion reveals that the surface associated with a revolute pair has

---

[8]We acknowledge Prof. Grigore Gogu of *Institut français de mécanique avancée*, Clemont-Ferrand, France, for bringing this work to our attention.

to be axially symmetric but cannot be extruded; the cylindrical surface is both. We should thus look for a generatrix $\mathcal{G}$ other than a straight line, but with G^2-continuity everywhere[9]. The latter would allow a shaft of appropriate diameter to be blended smoothly on both ends of $\mathcal{S}_R$. The simplest realization of the generatrix $\mathcal{G}$ of this surface is a polynomial $P(x)$ satisfying seven constraints, namely,

$$P(-1) = 0; \ P'(-1) = 0; \ P''(-1) = 0;$$
$$P(0) = 1; \ P(1) = 0; \ P'(1) = 0; \ P''(-1) = 0.$$

A sixth-degree polynomial is thus required to meet the above constraints. Solving for the coefficients, we obtain a 2-4-6 polynomial, namely, $P(x) = -x^6 + 3x^4 - 3x^2 + 1$.

Figure 10(a) shows a plot of $P(x)$ shifted by one unit upwards, with the purpose of allowing for the shaft with which $\mathcal{S}_R$ will blend, while Figure 10(b) is a 3D rendering of $\mathcal{S}_R$, the surface obtained by revolving the generatrix $\mathcal{G}$ about the x-axis, so as to blend with a cylinder of unit radius.

(a)   (b)

(c)
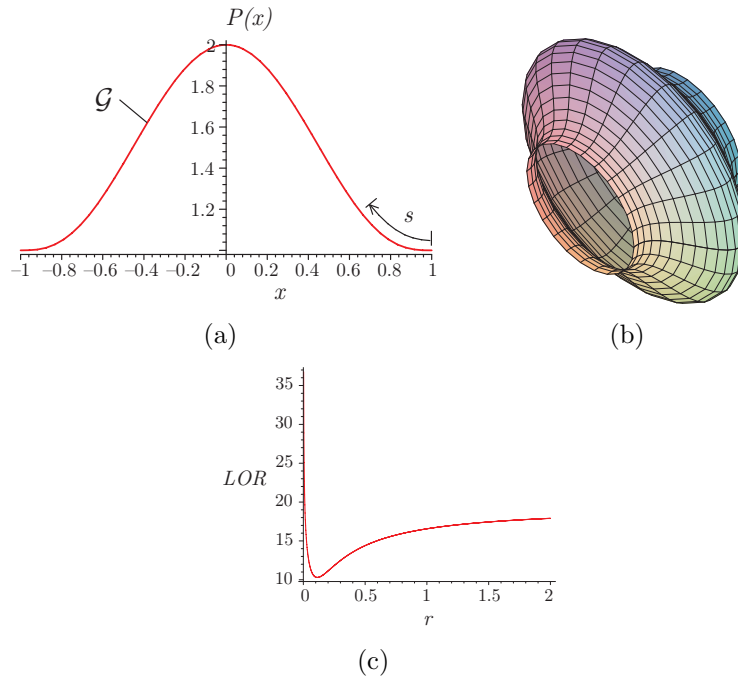
Figure 10: The simplest surface of revolution common to the two links coupled by a R joint: (a) a 3D rendering of the surface $\mathcal{S}_R$; and (b) its LOR vs. shaft radius r

The two principal curvatures of $\mathcal{S}_R$ are given as (Oprea, 2004)

$$\kappa_\mu = \frac{-y''}{(1 + y'^2)^{3/2}}, \quad \kappa_\pi = \frac{1}{y(1 + y'^2)^{1/2}} \tag{38}$$

---

[9]G^2-continuity of a surface means continuity of the surface itself, of its normal, and of its curvatures.

where $y = P(x) + r$ and r is the radius of the cylindrical shaft. The r.m.s. value of the two principal curvatures, κ_μ and κ_π, can now be obtained, namely,

$$\kappa_{rms} = \sqrt{\frac{y^2 y'' + (1 + y'^2)^2}{2(y^2(1 + y'^2)^3)}} \tag{39}$$

Next, we need to choose a suitable length parameter s and a homogenizing length l. A natural choice for s is the distance traveled along $\mathcal{G}$; l can be taken as the total length of the generatrix comprised within $-1 \le x \le 1$, the dimensionless parameter being $\sigma \equiv s/l$. In our case, $l = 2.9667$.

The LOR of $\mathcal{S}_\mathrm{R}$ can now be evaluated by eq.(2), and depicted in Fig. 10(c). Notice that LOR_R is not monotonic in r. Further, LOR_R reaches a minimum of 10.2999 at $r = 0.1132$. We thus assign $LOR_\mathrm{R} = 10.3$.

5.2   LOR of the Surface of the P Pair

The most common cross section of a P pair is a dovetail, but we might as well use an ellipse, a square or a rectangle. Or one could choose from a family of smooth curves, the *Lamé curves*, introduced in Subsection 4.4. This family continuously leads from a circle to a rectangle.

The LOR of the surface of the prismatic pair obtained by extruding a square or a rectangle is expected to have an unbounded value. A Lamé curve $\mathcal{L}$ with $m = 4$ is plausibly the best candidate for the cross section of the prismatic pair. This curve is shown in Fig. 11(a). Figure 11(b) is a 3D rendering of the surface $\mathcal{S}_\mathrm{P}$ obtained by extruding $\mathcal{L}$ along the z-axis.
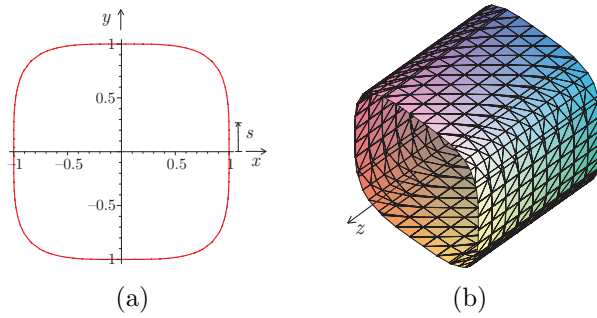
Figure 11: (a) Cross section of the prismatic pair; (b) A 3D rendering of the extruded surface $\mathcal{S}_\mathrm{P}$

The nonzero curvature of $\mathcal{S}_\mathrm{P}$ is given by

$$\kappa_\mu = \frac{x''y' - y''x'}{(x'^2 + y'^2)^{3/2}} \tag{40}$$

The r.m.s. value of the two principal curvatures thus reduces to $\kappa_{rms} = \kappa_\mu$. The length parameter s and the homogenizing length l are, correspondingly, the distance

traveled along $\mathcal{S}_\mathrm{P}$, depicted in Fig. 11(a), and the total length l of the Lamé curve, whence $\sigma \equiv s/l$. For the case at hand, $l = 7.0177$.

The loss of regularity LOR_P of $\mathcal{S}_\mathrm{P}$ is thus $LOR_\mathrm{P} = 19.6802$.

5.3   LOR of the Surface of the H Pair.

The surface $\mathcal{S}_\mathrm{H}$ associated with the helical pair can be obtained by sweeping a generatrix $\mathcal{G}_\mathrm{H}$ of a 2-4-6 polynomial—same as that used for the revolute pair—of "wavelength" λ along a helix of pitch p and radius r.
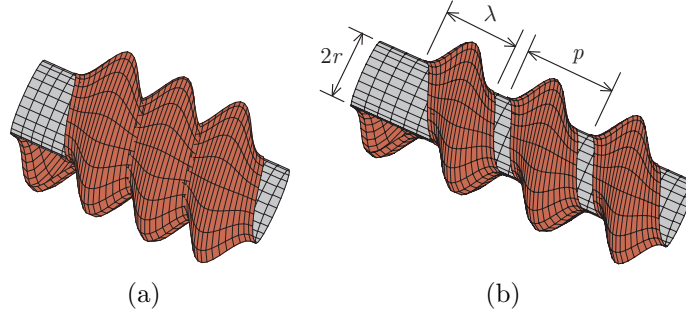
Figure 12: 3D rendering of a screw based on a 2-4-6 polynomial: (a) $p < \lambda$ (b) $p > \lambda$

Figure 12(a) shows a 3D rendering of the surface obtained when $p < \lambda$. Notice the presence of points with G^1 and G^2 discontinuities, forming a ridge. This set, describing a helix, is the intersection of the surface with itself. The LOR of the surface is thus infinite.

Figure 12(b) shows the 3D rendering of the surface obtained for $p > \lambda$, which exhibits G^2-continuity, and does so, in fact, for $p = \lambda$ as well. Figure 13(a) is a 3D plot of the LOR of the surface under study vs. $p/\lambda \geq 1.0$ and r/λ. By inspection, the minimum LOR lies along $p/\lambda = 1.0$. Figure 13(b) shows a plot of the LOR vs. r/λ for $p/\lambda = 1.0$, the LOR being minimum at $p/r \simeq 4.87$, with a value of $LOR_\mathrm{H} = 15.87017$.
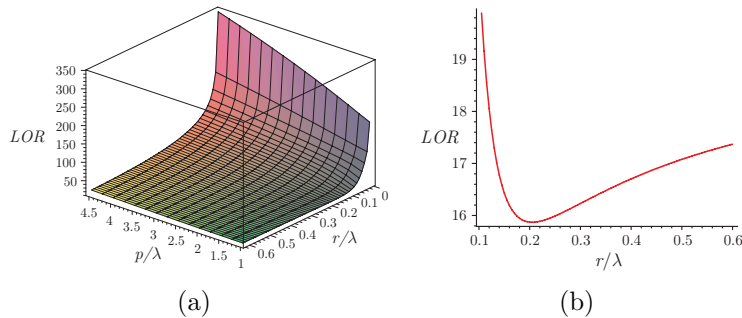
Figure 13: (a) 3D plot of LOR versus p/λ and r/λ ; (b) 2D plot of LOR versus r/λ for $p/\lambda = 1.0$

Finally, the LORs of the three elementary lower kinematic pairs are recorded in Table 1.

LKP	R	P	H
LOR	10.2999	**19.6802**	15.8702

Table 1: Loss of regularity of the three elementary LKPs

6   LOR of the Composite LKPs

While the composite LKPs have well-defined surfaces, namely, the cylinder, associated with the C pair, the plane, with the F pair, and the sphere, with the S pair, we do not resort to the LOR of these surfaces to obtain the complexity of these pairs. Indeed, these surfaces are too regular to fairly reflect the complexity associated with these pairs. Instead, we define the LOR of these pairs as the sums of the LORs of the elementary LKPs realizing them by means of a serial array. Furthermore, the realization of the composite pairs by means of elementary pairs can take various forms. To be fair, the realizations yielding the lowest LORs are chosen in the discussion below.

However, the geometric conditions to be obeyed by the elementary LKPs that realize their composite counterparts leads to the assemblability complexity of the LKPs, to be studied in Section 7.

6.1   The Cylindrical Pair

The cylindrical pair can be realized by means of a concatenation of a R pair with either a P or a H pair. Given that $\mathrm{LOR}_H < \mathrm{LOR}_P$, we would tend to choose the RH concatenation to realize this pair. However, this realization entails assemblability issues that are much more complex than those brought about by the alternative realization by means of a R and a P pairs. Indeed, the RH serial array calls for the laying out of the axes of the two pairs along the same line, which adds to the complexity of this realization. The LOR in question is, thus,

$$\mathrm{LOR}_C = \mathrm{LOR}_R + \mathrm{LOR}_P = 29.9801 \tag{41a}$$

6.2   The Planar Pair

The planar pair can be realized by means of a concatenation of a combination of three pairs, namely, RRR, PRR, RPR, RRP, PPR, PRP, RPP, where all R pairs are of parallel axes and the P pair is of direction parallel to the axis of the R pair(s) involved. Given that $\mathrm{LOR}_R < \mathrm{LOR}_P$, we choose the RRR concatenation to realize this pair, which then yields

$$\mathrm{LOR}_F = 3 \times \mathrm{LOR}_R = 30.8997 \tag{41b}$$

6.3   The Spherical Pair

The spherical pair can only be realized by means of three R pairs of concurrent axes, and hence,

$$\text{LOR}_S = 3 \times \text{LOR}_R = 30.8997 \tag{41c}$$

6.4   The Shape Complexity of the LKPs

The shape complexity $K_{S|x}$ of the six LKPs can now be defined as a normalized LOR, namely, as

$$K_{S|x} = \frac{\text{LOR}_x}{\text{LOR}_{max}}, \quad \text{LOR}_{max} = \text{LOR}_F = \text{LOR}_S = 30.8997 \tag{42}$$

Table 2 summarizes the shape complexity of all six LKPs.

LKP	R	P	H	C	F	S
$K_{S|x}$	0.3333	0.6369	0.5136	0.9702	1.000	1.000

Table 2: Shape complexity of the six elementary lower kinematic pairs

7   Joint-assemblability Complexity of the LKPs

The LOR of the composite pairs, however, does not reflect completely the complexity of these pairs. For example, their LOR does not tell the complexity difference between the planar pair and its spherical counterpart. That is, the LOR of these pairs does not consider the complexity involved in the parallelism or concurrency condition between joint axes. It is thus necessary to factor this complexity into the overall complexity of these pairs.

What is at stake here is the requirements imposed by the suitable laying out of the individual elementary pairs making up a composite pair. These requirements bring about a complexity due to the assemblability of the joint in question. Hence the name given to this complexity measure: *joint-assemblability complexity*, to distinguish it from *linkage-assemblability complexity*, to be introduced presently. The complexity of interest to this section will thus be represented by $K_{J|x}$, where x denotes the type of pair at stake, C, F or S. Notice that the elementary pairs not having any assemblability issues, they will be assigned a $K_{J|x}$ of zero.

7.1   The Cylindrical Pair

Assemblability of this pair requires that the axis of the R pair be parallel to the direction of the P pair—this pair, it is recalled, does not have an axis. Let the axis

of the R pair be parallel to the unit vector $\mathbf{e}_1$, the direction of the P pair being given by $\mathbf{e}_2$. The parallelism condition then takes the form

$$\mathbf{e}_1 \times \mathbf{e}_2 = \mathbf{0} \tag{43}$$

Upon expansion, each of the three components of the left-hand side of the above equation apparently involves one addition (A) and two multiplications (M), the cross product thus involving a computational complexity of $3A + 6M$, or six flops—a flop, abbreviation of *floating-point operation*, is defined as one addition and one multiplication.

　　Notice that, if the cylindrical pair is realized with the series layout of a R and a H pair, then the assemblability condition requires that the axes of the two pairs coincide. As the coincidence condition requires the vanishing of three product vectors (Angeles, 1998), the assemblability requirement of these two pairs is thus three times that of the RP layout.

7.2　The Planar Pair

The planar pair F can be realized most simply by means of a serial array of three R pairs of parallel axes. Let the axis of the ith R pair be $\mathcal{A}_i$, of direction given by the unit vector $\mathbf{e}_i$, for $i = 1, 2, 3$. The geometric constraint imposed by the realization of the planar pair reduces then to the parallelism of the three foregoing unit vectors, which then takes the form

$$\mathbf{e}_1 \times \mathbf{e}_2 = \mathbf{0} \quad \text{and} \quad \mathbf{e}_2 \times \mathbf{e}_3 = \mathbf{0} \tag{44}$$

The computational complexity of the realization of the F pair thus reduces to 12 flops.

7.3　The Spherical Pair

The only possible realization of the S pair is via a series array of three revolutes of concurrent axes. Let the ith axis $\mathcal{A}_i$ in question be defined by a point A_i, of position vector $\mathbf{a}_i$, and a direction given by the unit vector $\mathbf{e}_i$, for $i = 1, 2, 3$. The realization of the spherical pair requires that the three lines intersect at a common point O, which, without loss of generality, can be taken as the origin of the three-dimensional vector space. The *moment* of $\mathcal{A}_i$ with respect to O is defined in *line geometry* (Pottman and Wallner, 2001) as $\mathbf{m}_i = \mathbf{e}_i \times \mathbf{a}_i$. The condition that the line passes through point O then requires that $\mathbf{m}_i = \mathbf{0}$, the concurrence of the three lines at point O then reducing to the vanishing of the three foregoing moments, which then takes the form

$$\mathbf{e}_1 \times \mathbf{a}_1 = \mathbf{0}, \quad \mathbf{e}_2 \times \mathbf{a}_2 = \mathbf{0} \quad \text{and} \quad \mathbf{e}_3 \times \mathbf{a}_3 = \mathbf{0} \tag{45}$$

The computational complexity of the realization of the S pair thus amounts to 18 flops.

7.4   Summary of Joint-assemblability Complexity

The joint-assemblability complexity $K_{J|x}$ of the LKPs is now defined as the ratio of the number of flops required by the constraint imposed on their realization divided by the foregoing maximum number of flops, which is 18. Therefore, if we recall that the $K_{J|x}$ values of the elementary pairs was defined as zero,

$$K_{J|R} = K_{J|P} = K_{J|H} = 0, \quad K_{J|C} = \frac{1}{3}, \quad K_{J|F} = \frac{2}{3}, \quad K_{J|S} = 1 \qquad (46)$$

8   Joint-type Complexity of the Six LKPs

The *joint-type complexity* $K_{T|x}$ of the six LKPs is now defined as the mean value of their shape and joint-assemblability complexity measures, whence the complexity values of Table 3 are derived.

LKP	R	P	H	C	F	S
$K_{T|x}$	0.1667	0.3185	0.2568	0.6518	0.8333	1.000

Table 3: Joint-type complexity of the six elementary lower kinematic pairs

9   Complexity of Simple Kinematic Chains

Three aspects of complexity can be associated with simple kinematic chains: *linkage-assemblability*; *joint-type*; and *link-morphology diversity*. The complexity of simple kinematic chains is then defined as the mean value of these three partial-complexity measures.

9.1   Linkage-assemblability Complexity (LAC)

This type is proper of *overconstrained chains*, i.e., simple closed chains with what is known as *reduced* or *lower mobility*. We consider here only planar, spherical and Schönflies chains. The first two are well known, the third type is less so. Schönflies chains are those involving displacements of the Schönflies subgroup (Hervé, 1999), most commonly produced by what is known as SCARA (Selective Compliance Assembly Robot Arm) systems. These systems are capable of producing three independent translations and one rotation about an axis of fixed direction.

Linkage-assemblability relates to the requirement that the various axes involved obey parallelism or concurrency conditions, similar to joint-assemblability.

The LAC of planar chains stems from the condition that all the kinematic pairs of the chain have parallel axes[10]. If the chain has N LKPs, then $N - 1$ parallelism

---

[10]P pairs not having an axis, only a direction is included here, with the provision that the discussion, in this case, pertains to their motion-direction.

conditions identical to those of Subsection 7.2 must be observed, and hence, the number of flops N_{LPl} associated with this type of chains is

$$N_{LPl} = 6(N - 1) \tag{47}$$

The LAC of spherical chains lies in the requirement that all axes of their N R joints be concurrent at one common point. In this case N concurrency conditions identical to those of Subsection 7.3 must be observed, the number of flops N_{LSph} associated with this type of chains thus being

$$N_{LSph} = 6N \tag{48}$$

A simple kinematic chain of the Schönflies type can have a number N of a combination of R, H and P joints, the same provision as that pertaining to planar chains applying to P joints here. In Subsection 7.1 we saw that, although the screw pair has a shape complexity lower than the P chain, the assemblability of the latter with a R pair to produce a C pair is much simpler than if the former were used, and hence, the C chain was regarded as a serial RP (or PR) layout. Likewise, in this case we regard the Schönflies chain as being a layout of R and at least one P joints, with the R joints of parallel axes and the P joints of direction parallel to the former. In this case, then, $N - 1$ parallelism conditions are to be obeyed, the total number of flops associated with these chains then being

$$N_{LSch} = 6(N - 1) \tag{49}$$

The LAC $K_{L|x}$ of the chains under study can now be defined as the ratio of the corresponding number of flops divided by the maximum, which is, apparently, $6N$. Therefore,

$$K_{L|Pl} = K_{L|Sch} = 1 - \frac{1}{N}, \quad K_{L|Sph} = 1 \tag{50}$$

Plausibly, as the number of links of the planar and Schönflies chains grows, their complexity grows correspondingly. However, the complexity of spherical chains remains unity. Nevertheless, notice that the foregoing analysis applies only to closed chains, the universal (U) joint being a two-dof open chain thus being excluded. The assemblability complexity of this layout can be regarded as that of a joint not included among the six LKPs. The reason here is that this joint does not have a surface associated with it. If we resort to the approach taken to define the joint-assemblabilty complexity of this chain, then we have two zero-moment conditions of the type introduced in Subsection 7.3 to meet, and hence,

$$K_{J|U} = \frac{2}{3} = 0.6667 \tag{51a}$$

The shape complexity of the U-joint is the normalized sum of the LORs of its two R joints, i.e.,

$$K_{S|U} = 0.6667 \tag{51b}$$

Therefore, the type complexity of the U-joint is the mean value of the two foregoing complexity values, namely,

$$K_{T|U} = 0.6667 \tag{51c}$$

9.2 Joint-type Linkage Complexity (JLC)

Let a simple kinematic chain be composed of n_x joints of the x-type, where x stands for R, P, H, C, F, S, and, for completeness, U. Let, moreover, the total number of joints be n. The JLC K_{JL} of the joint is then the weighted mean of the partial complexity values of the various joint types, i.e.,

$$K_{JL} = \frac{1}{n}(n_R K_{T|R} + n_P K_{T|P} + n_H K_{T|H} + n_C K_{T|C} + n_F K_{T|F}$$
$$+ n_S K_{T|S} + n_U K_{T|U}), \quad n = n_R + n_P + n_H + \ldots + n_U \tag{52}$$

where n_R, n_P and n_H are the numbers of revolute, prismatic, and helical joints, respectively, while $K_{T|x}$ is the type complexity of the pair x as recorded in Table 3.

9.3 Link-morphology Diversity (LMD)

At the qualitative-synthesis stage, only partial information about the geometric relations between neighboring joints is available. However, this information suffices to allow the linkage designer to distinguish five possible binary-link morphologies, displayed in Fig. 14, as the relative layout between its two joint axes defines such a link[11]. In this light, *unary* links, i.e., those coupled to only one single link, do not contribute to the LMD K_{LM} of the chain. Moreover, as composite joints can be considered as concatenations of elementary joints, only the latter need be considered.

Helical, like revolute joints, bear an axis. Hence, the set of the possible link morphologies in a kinematic chain containing revolute as well as helical joints shown in Fig. 14 can be conveniently applied in the presence of helical joints as well.

Prismatic joints, on the other hand, have only a direction, but no axis. In the presence of a prismatic joint, intersection does not apply. The only morphological relations between either a R and a P pairs or two P pairs is whether parallelism or perpendicularity exist; if none of these, then the relation at stake is an arbitrary layout. The selection should be made, however, to keep the link diversity to a minimum.

In order to define the link-morphology diversity of the linkage under study, the concept of *entropy* from *molecular thermodynamics* and from *information theory* is recalled. In this vein, the LMD, or link-morphology complexity for that matter, is defined as:

$$K_{LM} = \frac{M}{M_{max}} \tag{53}$$

---

[11]Ternary and higher-order links can be accommodated, but the discussion of these links is left aside because of the scope of the paper.
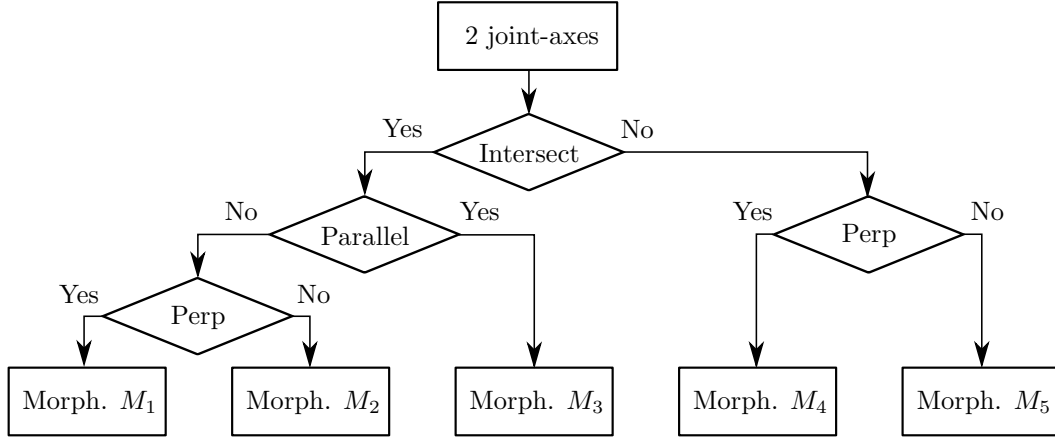
Figure 14: Binary tree displaying possible link morphologies

where M is the entropy of the link morphologies, M_{max} being the maximum possible value of M. If we let N_i be the number of instances of M_i and L the number of links of the chain, then we have

$$M = -\sum_{i=1}^{5} m_i \log_2(m_i); \quad m_i = \frac{M_i}{L}, \quad L \equiv \sum_{i=1}^{5} M_i \tag{54}$$

M is known to attain its maximum when all the above five morphologies occur with equal frequency (Luenberger, 1984). In this case, $m_1 = m_2 = \ldots = m_5 = 1/5$, which then leads to

$$M_{max} = -\sum_{i=1}^{5} \frac{1}{5} \log_2\left(\frac{1}{5}\right) = \log_2(5) = 2.3219 \text{ bits} \tag{55}$$

Moreover, M attains its minimum when all links bear the same morphology. Without loss of generality, one can assume here that M_1 is the morphology in question, which leads to $m_1 = 1$ and $m_2 = \ldots = m_5 = 0$, the outcome being that

$$M_{min} = -M_1 \log_2(M_1)\left.\right|_{M_1=1} - \lim_{x \to 0}\left[\sum_{i=2}^{5} x \log_2(x)\right] = 0 + 0 = 0 \tag{56}$$

Hence, $0 \leq M \leq 1$, which is the range of values of a complexity measure, as adopted at the outset.

9.4   Summary of Complexity of Simple Kinematic Chains

The complexity of a simple kinematic chain is now evaluated as the mean value of the three partial complexity measures defined above: i) joint-type complexity K_J, ii) linkage assemblability K_L and iii) link-morphology diversity K_M, i.e.,

$$K = \frac{1}{3}(K_J + K_L + K_M) \tag{57}$$

10 Examples

10.1 Example 1: The Four-bar Linkage

In order to evaluate the complexity of a linkage we use expression(57). We have, for all three versions, $N = 4$:

10.1.1 Planar Four-bar Linkage

In this case, only R pairs occur, all of parallel axes, and hence,

$$K_J = \frac{1}{4}4K_{T|R} = K_{T|R} = 0.1667 = \frac{1}{6}$$

$$K_L = K_{L|Pl} = 1 - \frac{1}{4} = \frac{3}{4}$$

$$K_M = 0$$

Therefore,

$$K = \frac{1}{3}\left(\frac{3}{4} + \frac{1}{6}\right) = \frac{11}{36} = 0.3056$$

10.1.2 Spherical Four-bar Linkage

Again, only R pairs occur here, all of concurrent axes, whence,

$$K_J = \frac{1}{4}4K_{T|R} = K_{T|R} = 0.1667 = \frac{1}{6}$$

$$K_L = 1$$

$$K_M = 0$$

Thus,

$$K = \frac{1}{3}\left(1 + \frac{1}{6} + 0\right) = 0.3839$$

10.1.3 Spatial Four-bar Linkage

This is a linkage of the RCCC type, with all joints of arbitrary layout and all links of arbitrary morphology. Moreover, this version, contrary to the previous ones, is isostatic, i.e., non-overconstrained, whence, its LAC vanishes. Therefore,

$$K_J = \frac{1}{4}(0.1667 + 3 \times 0.2568) = 0.2343$$

$$K_L = 0$$

$$K_M = 0$$

Hence,

$$K = \frac{1}{3}(0 + 0.2343 + 0) = 0.0781$$

Therefore, the most complex of the three foregoing linkages is the spherical version, followed by the planar, the simplest being the spatial version. This result is plausible, as producing four revolute joints of concurrent axes is more challenging than producing four of parallel axes. The spatial version being the most tolerant, it is bound to be the simplest version.

10.2 Example 2: Transmission of Vertical into Horizontal Rotation

This example pertains to the qualitative synthesis of a linkage needed to transform the vertical rotation of a motor axis into the horizontal rotation of a load. The motivation here is the design of a two-degree-of-freedom pan-tilt generator. This mechanical transmission, shown in Fig. 15, comprises two input angular velocities, as produced by corresponding motors, ω_R of the ring gear and ω_S of the sun gear of a planetary gear train. The output angular velocities are associated with the pan and the tilt rotations. The pan rotation is simply that of the planet-carrier, the tilt rotation that of the planet gears, which is to be converted from vertical into horizontal. Moreover, in order to a) best use the power available and b) overconstrain the planetary train to reduce backlash, it is desired that the two planets drive the single tilt shaft of the load link. Furthermore, although the angular velocity ratio from the planet gears to the tilt shaft might as well be a constant 1:1, slight deviations from this constant ratio are accepted, as the linkage will operate under computer control. Deviations from the constant velocity ratio will be compensated for by means of a kinematic control algorithm, which need not be discussed here.

The design team has come up with three conceptual solutions, as a result of brainstorming sessions: *i*) a double universal joint, each with input and output angles at 45°; *ii*) a five-bar linkage of the RHRRR type; and *iii*) a spherical four-bar linkage. The three alternative solutions are analyzed below in terms of their kinematic complexity.

10.2.1 Double Universal Joint (DUJ)

This linkage, depicted in Fig. 16, can be analyzed as a simple kinematic chain of the RUUR type, which can be regarded as one more version of the four-bar linkage. However, this four-bar linkage does not fall within those studied in the Subsection 9.1 because its LAC cannot be reduced to one common parallelism or concurrency condition. We analyze here this chain as composed of six R joints, with pairwise intersecting axes.

As the chain involves three pairs of R joints with intersecting axes, and each intersection is represented with six flops, as per Subsection 7.3, the total number of
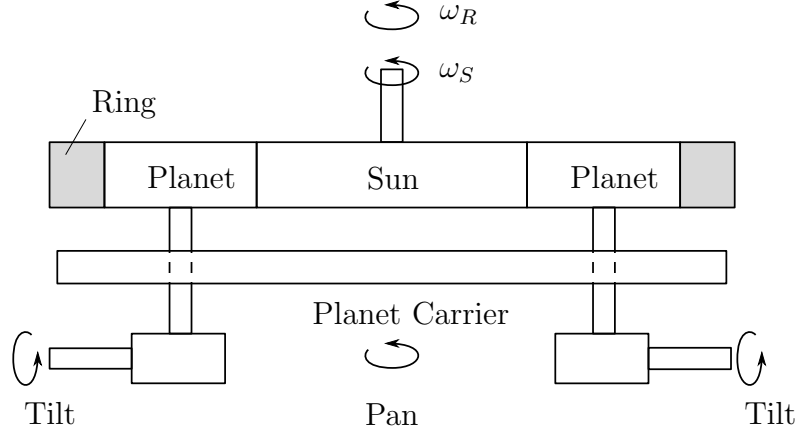
Figure 15: The general layout of a pan-tilt generator, showing its two input angular velocities, ω_R and ω_S, and its pan and tilt output angular velocities
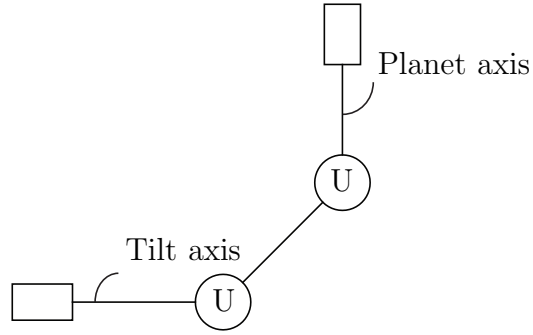

Figure 16: A schematic of the double universal joint converting rotation about a vertical into rotation about a horizontal axis

flops required to represent the three intersections is

$$N_{LDUG} = 3 \times 6 = 18$$

and, since the number of links is $N = 6$, the LAC of the DUJ is

$$K_{LDUG} = \frac{N_{LDUG}}{6N} = \frac{18}{36} = \frac{1}{2}$$

Moreover, the joint-type complexity of the chain is obtained from expression(52), upon regarding the chain as one of type RUUR, i.e.,

$$K_J = \frac{1}{4}\left(2K_{T|R} + 2K_{T|U}\right) = \frac{1}{2}\left(K_{T|R} + K_{T|U}\right) = \frac{5}{12} = 0.4167$$

Finally, to compute the link-morphology diversity, the chain is regarded as a six-bar linkage with a symmetric morphology: the intermediate link, known as the Cardan

shaft, bears two R joints of parallel axes, all other five links bearing two R joints of axes intersecting at right angles. That is, the double universal joint comprises links of two distinct morphologies, M_1 and M_3, with $m_1 = 5/6$ and $m_3 = 1/6$, all other m_i values vanishing. Hence, the link-morphology diversity of the linkage is

$$M = -\left[\frac{5}{6}\log_2\left(\frac{5}{6}\right) + \frac{1}{6}\log_2\left(\frac{1}{6}\right)\right] = 0.6501$$

whence,

$$K_M = \frac{0.6501}{2.3219} = 0.2800$$

Therefore, the kinematic complexity of the UU joint is

$$K = \frac{1}{3}(0.5000 + 0.4167 + 0.2800) = 0.3989$$

10.2.2   Five-bar Linkage

The linkage is question is depicted in Fig. 17. It consists of one first R pair coupled to the frame 0 that is followed by a H pair coaxial with the foregoing R joint, the balance three R joints being of parallel axes, and normal to the common axis of the first two joints. The five-bar linkage thus resulting is overconstrained, the determination of its degree of freedom being elusive to the usual Chebyschev-Grübler-Kutzbach formula, but tractable using the theory of groups propounded by Hervé (1999), which yields a dof of unity.

Because of the overconstrained nature of the linkage, its LAC is different from zero. Moreover, as this linkage does not fall into any of the three types studied in Subsection 9.1, its complexity will have to be evaluated on an ad-hoc basis: to ease this evaluation, the RH layout is replaced by a C joint, while the RRR layout by a F pair, thereby ending up with a CF linkage. The number of flops required to describe the assemblability requirements thus involves: a) those of the C pair, 6, as this entails one cross product; b) those of the F pair, $6 \times (3 - 1) = 12$; and c) a dot product, required to realize the perpendicularity of the axis of the C pair with the plane of the F pair, thereby adding 3 flops. The total number of flops in question is, thus, $N_f = 21$. As the maximum number of flops found in Subsection 9.1 was $6N$, we have, with $N = 5$, $N_{max} = 30$, and hence,

$$K_L = \frac{21}{30} = \frac{7}{10} = 0.7000$$

The joint-type complexity of the chain is, in turn, the mean value of the complexities of the four R joints and the single H joint, i.e.,

$$K_J = \frac{1}{5}\left(4 \times \frac{1}{6} + 0.2568\right) = 0.9235$$

As the chain involves one link, the frame, with offset axes oriented at right angles (M_4 morphology), we have $m_4 = 1/5$. Moreover, one chain link, number 1, is of the M_3 morphology, while link number 2 is of the M_1 morphology, the balance two links being of M_3 morphology as well. In summary, then, $m_1 = 1/5$, $m_2 = 0$, $m_3 = 3/5$, $m_4 = 1/5$, $m_5 = 0$. Therefore,

$$M = -\left[\frac{1}{5}\log_2\left(\frac{1}{5}\right) + \frac{3}{5}\log_2\left(\frac{3}{5}\right) + \frac{1}{5}\log_2\left(\frac{1}{5}\right)\right] = 1.3710$$

whence,

$$K_M = \frac{1.3710}{2.3219} = 0.5905$$

Thus, the overall kinematic complexity of the chain under study is

$$K = \frac{1}{3}(0.7000 + 0.9235 + 0.5905) = 0.7380$$

10.2.3   Spherical Four-bar Linkage

A spherical four-bar linkage with input and output axes at right angles can be synthesized so as to produce an input-output velocity relation "close to" 1:1, if linkage synthesis techniques are used for function generation (Chiang, 1988). Here we are interested only on the qualitative complexity of this linkage. In Example 1 the kinematic complexity of a *generic* spherical four-bar linkage was already computed. For the *specific* linkage at hand we have to include the complexity associated with the condition that the input and output axes intersect at right angles, which brings about one morphology of the M_1 type, all other being of the M_2 type. Hence, the LMD of the linkage of interest, obtained for the generic spherical four-bar linkage in Example 1 as 0, will have be modified, to yield

$$M = -\left[\frac{1}{4}\log_2\left(\frac{1}{4}\right) + \frac{3}{4}\log_2\left(\frac{3}{4}\right)\right] = 0.6038$$

whence,

$$K_M = \frac{0.6038}{2.3219} = 0.2600$$

The other complexity values associated with the spherical four-bar linkage, as obtained in Example 1, are reproduced below for quick reference:

$$K_L = 1, \quad K_J = 0.1667$$

Therefore, the overall kinematic complexity of the four-bar linkage at hand is obtained as

$$K = \frac{1}{3}(1 + 0.1667 + 0.2600) = 0.4756$$

In summary, then, of the three alternative solutions proposed, the double universal joint is the simplest one, followed by the spherical four-bar linkage, the five-bar linkage being the most complex.
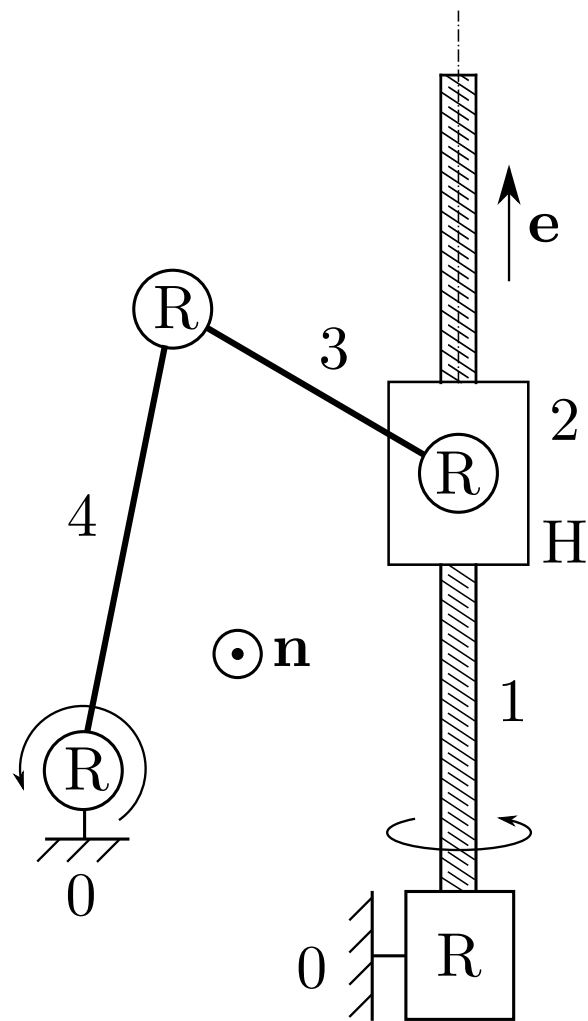
Figure 17: A schematic of the RHRRR five-bar linkage.

11   Conclusions

In this paper a novel index, the loss of regularity, was used to assign a complexity value to curves and surfaces. A few propositions on the concept of loss of regularity were proven. The concept was then illustrated with various examples of planar curves. Next, for the elementary lower kinematic pairs, a minimum-LOR paradigm surface was proposed. The LOR associated with the composite LKPs was found as the sum of the LORs of their simplest realizations with serial arrays of elementary LKPs. Derived from the LORs of the six LKPs was the shape complexity of these chains which, together with their assemblability complexities, yield the joint-type complexity of the six LKPs. The complexity of simple kinematic chains was proposed as the mean value of three partial complexity measures: linkage-assemblability; joint-type; and link-morphology diversity. Various examples illustrates the application of complexity to the qualitative synthesis of simple kinematic chains.

12   Acknowledgements

References

Angeles, J. 1998. The application of dual algebra to kinematic analysis", in Angeles, J. and Zakhariev, E. (editors), Computational Methods in Mechanical Systems, Springer-Verlag, Heidelberg, Vol. 161, pp. 3–31.

Burmester, L., 1888, *Lehrbuch der Kinematik*, Arthur Felix Verlag, Leipzig, Germany.

French MJ. Insight, design principles and systematic invention. In: Chakrabarti A, editors. Engineering design synthesis: understanding, approaches and tools, London: Springer; 2002, p. 19–34.

Chiang, C.H., 1988. Kinematics of Spherical Mechanisms. Cambridge University Press, Cambridge.

Courant R, Hilbert D. Methods of mathematical physics. New York: Interscience Publishers; 1953.

Freudenstein, F., 1955, "Approximate synthesis of four-bar linkages" *Trans. ASME*, Vol. 77, pp. 853–861.

Gardner M. The superellipse: a curve that lies between the ellipse and the rectangle. Scientific American 1965;213:222–34.

Garey MR, Johnson DS. Computers and intractability: A guide to the theory of NP-completeness. New Jersey: Bell Laboratories: 1979.

Gibson CG. Elementary geometry of algebraic curves. Cambridge: Cambridge University Press; 1998.

Hartenberg RS, Denavir J. Kinematic synthesis of linkages. New York: McGraw-Hill; 1964.

Hervé J. The Lie group of rigid body displacements, a fundamental tool for mechanical design. Mech. Mach. Theory 1999;34:719–30.

Jaklič A, Leonardis A, Solina F. Segmentation and recovery of superquadrics. Dordrecht: Kluwer Academic Publishers; 2000.

Khan WA, Caro S, Pasini D, Angeles J. Complexity-Based Rules for the Conceptual Design of Robotic Architectures. in Lenarčič, J. and Roth, B. (editors), *On Advances in Robot Kinematics* 2006, Springer, Dordrecht, pp. 359–368.

Khan WA, Caro S, Pasini D, Angeles J. A Formulation of Complexity Based rules for the Preliminary Design Stage of Robotic Architectures. The International Conference on Engineering Design, August 28–31, 2007, Paris, France.

Koenderink JJ. Solid shape. Cambridge: MIT Press; 1990.

Li M, Vitányi P. An introduction to Kolmogorov complexity and its applications. 2nd ed. New York: Springer-Verlag; 1997.

Loria G. Spezielle algebraische und transscendente ebene Kurven: Theorie und Geschichte. Leipzig: BG Teubner; 1902.

Luenberger DG. Linear and Nonlinear Programming. 2nd ed. Reading (MA): Addison-Wesley Publishing Company; 1984.

Oprea J. Differential geometry and its applications. New Jersey: Pearson Prentice Hall; 2004.

Pottmann, H. and Walner, J. Computational Line Geometry. Berlin-Heidelberg-New York: Springer; 2001.

Rossignac J. Shape complexity. The Visual Computer 2005;21–12:985–96.

Shigley JE, Mischke CM. Mechanical engineering design. 5th ed. New York: McGraw-Hill Book Company; 1989.

Strang G. Introduction to applied mathematics. Cambridge (MA): Wesley-Cambridge Press; 1986.

Taguchi G. Taguchi on robust technology development. Bringing quality engineering upstream. New York: ASME Press; 1993.

Voinea RP, Stroe IV. A general method for kinematic pairs synthesis. Mech. Mach. Theory 1995;30–3:461–70.

Walsh PJ. A polynomial time complexity bound for computations of curves. SIAM Journal on Computing 1998;28–2:704–8.